LA-UR- 11-05327

*Approved for public release; distribution is unlimited.*

*Title:* The evolution of solid density within a thermal explosion I. Proton radiography of pre-ignition expansion, material motion and chemical decomposition

*Author(s):* Laura Smilowitz, Bryan F. Henson, Jerry J. Romero, Blaine W Asay, Andy Saunders, Frank E. Merrill, Chris Morris, Kris Kwiatkowski, Gary P. Grim, Fassah Marriam, Cindy Schwartz, Gary Hogan, Paul Nedrow, Mathew Murray, Niel Thompson, Camilo Espinoza, Doug Lewis, Joe Bainbridge, Wendy McNeil, Mark Marr-Lyon and Paul Rightly

*Intended for:* Journal of Applied Physics

Los Alamos
NATIONAL LABORATORY
EST. 1943

Los Alamos National Laboratory, an affirmative action/equal opportunity employer, is operated by the Los Alamos National Security, LLC for the National Nuclear Security Administration of the U.S. Department of Energy under contract DE-AC52-06NA25396. By acceptance of this article, the publisher recognizes that the U.S. Government retains a nonexclusive, royalty-free license to publish or reproduce the published form of this contribution, or to allow others to do so, for U.S. Government purposes. Los Alamos National Laboratory requests that the publisher identify this article as work performed under the auspices of the U.S. Department of Energy. Los Alamos National Laboratory strongly supports academic freedom and a researcher's right to publish; as an institution, however, the Laboratory does not endorse the viewpoint of a publication or guarantee its technical correctness.

Form 836 (7/06)

# The evolution of solid density within a thermal explosion I. Proton radiography of pre-ignition expansion, material motion and chemical decomposition

L. Smilowitz, B. F. Henson, J. J. Romero, B. W. Asay, A. Saunders, F. E. Merrill, C. L. Morris, K. Kwiatkowski, G. Grim, F. Mariam, C. L. Schwartz, G. Hogan, P. Nedrow, M. M. Murray, T. N. Thompson, C. Espinoza, D. Lewis, J. Bainbridge, W. McNeil, P. Rightley and M. Marr-Lyon

*Los Alamos National Laboratory*
*Los Alamos, NM 87545*

PACS numbers: 82.33.Vx; 25.40.Cm; 82.30.Lp; 82.40.-g

**ABSTRACT**

We report proton transmission images obtained during direct heating of a sample of PBX 9501 (a plastic bonded formulation of the explosive nitramine octahydro-1,3,5,7-tetranitro-1,3,5,7-tetrazocine (HMX)) prior to the ignition of a thermal explosion. We describe the application of proton radiography using the 800 MeV proton accelerator at Los Alamos National Laboratory to obtain transmission images in these thermal explosion experiments. We have obtained images at two spatial magnifications and viewing both the radial and transverse axis of a solid cylindrical sample encased in aluminum. During heating we observe the slow evolution of proton transmission through the samples, with particular detail during material flow associated with the HMX $\beta$-$\delta$ phase transition. We also directly observe the loss of solid density to decomposition associated with elevated temperatures in the volume defining the ignition location in these experiments. We measure a diameter associated with this volume of 1-2 mm, in agreement with previous measurements of the diameter using spatially resolved fast thermocouples.

## I. INTRODUCTION

Most of what is known about the thermal behavior of a solid explosive like PBX 9501 is determined from measurements of the material in conditions that inhibit the explosive response. The material properties at elevated temperature are studied using very small quantities, unconfined, coupled to a good thermal conductor, and using such standard analytical probes as differential scanning calorimetry (DSC), thermogravimetric analysis (TGA), linear expansion, thermal conductivity, etc. This is necessary in order to protect the equipment from the damage caused by an explosion. Another means for studying the properties of thermally damaged explosives is to heat them to a point below the ignition event, and then cool them in an attempt to quench the material state in the conditions of the highest temperature achieved. This allows larger samples and confined geometries, but necessitates ceasing the heating prior to ignition and assuming that there are no changes in state upon cooling. While these two approaches are useful, both suffer limitations with regard to understanding the behavior of the material under the conditions which would give rise to a thermal explosion. Inherently, by restricting the feedback of thermal and chemical energy to the solid to prevent a thermal explosion, the material is not experiencing the same conditions as those that would lead to such an event.

In this paper, we report the application of a fast radiographic technique to obtain density images within a solid thermal explosion using the Proton Radiographic (pRad) facility at Los Alamos National Laboratory. This tool allows us to image the material *in situ* as it is heated to thermal explosion in a fully confined geometry. The experiments were performed on solid cylindrical samples of an HMX based explosive formulation PBX 9501 encased in aluminum. By direct heating applied to the cylindrical case we generate a nonlinear thermal ignition at the center of the sample. Using asynchronous proton transmission images obtained during heating

we measure material expansion during heating, material expansion and flow caused by a crystallographic transformation between the β and δ phases of HMX[1, 2] and the loss of mass to decomposition at the location of the thermal runaway and ignition. Application of proton pulses synchronized to the ignition event to image the consumption of solid by burning during the explosion has been briefly described elsewhere,[3] and will be more fully described in a companion paper in this journal.[4]

## II. EXPERIMENTAL

### A. Proton beam details

Transmission images are obtained using the 800 MeV proton accelerator at Los Alamos National Laboratory. The proton beam is delivered as macropulses of 800 μs duration at 20 Hz.[5] Within the macropulse, individual proton pulses are spaced at 5 ns and are delivered with adjustable duration and inter-pulse times with 5 ns increments. The accelerator is a very high flux source, and intensity is attenuated in these experiments giving a nominal sample transmission of 60 - 80%. The proton beam is focused using either of two quadropolar magnet configurations to create an image plane. The two magnet configurations yield lenses of either 1x magnification, with a full field of 100 x 100 mm and spatial resolution of 100 μm, or 3x magnification, with a full field of 40 x 40 mm and spatial resolution of 70μm.

The sample is illuminated in this plane and the spatially resolved transmission through the sample converted to optical luminescence with a Ce doped $Lu_2SiO_5$ (LSO) scintillator material and recorded by digital framing cameras. Recorded images were digitally processed to normalize against the proton beam intensity and spatial variability. Both absolute transmission

images, and images of the change in transmission, normalized against static images, were used in the analysis.

Contrast and variation in the transmission of protons through the sample are a function of the material density and transmission path length. The product of density and path length is the sample areal density. Measured proton transmission may be converted to sample areal density using a transmission model based on measured proton-target nuclear interactions and multiple Coulomb scattering. The transmission and areal density characteristics of the experiments reported here are shown in Fig. 1. In Fig 1A the percent transmission of the beam through the samples as a function of the total areal density are plotted for both the identity and x3 magnification configurations, where the transmission difference is due to different collimator configurations. In Fig. 1B the transmission normalized to a static image of the experiment is shown as a function of the change in explosive areal density, again for both imaging configurations.

## B. Radial thermal explosion

The high explosive (HE) sample consists of two right circular cylinders of PBX 9501 12.7 mm (1/2") in diameter by 12.7 mm in height for the small geometry and 25.4 mm in diameter by 12.7 mm in height for the large geometry. Two samples are joined along the cylinder axis to form a single 2 to 1 aspect ratio (small) or 1 to 1 aspect ratio (large) cylinder which is encased in aluminum 3.2 mm (1/8") thick along the cylinder wall with endcaps approximately 3.2 mm thick. The sample and case are assembled as two halves defining a midplane in the sample. Fine gauge thermocouples (75 micron wire) and a 200 μm core diameter optical fiber are introduced through the case at this midplane. The assembled halves are glued at the case to seal

the sample and the endcaps are compressed by external bolts anchored in the endcaps. A drawing of the full sample configuration for the 1" diameter by 1" tall configuration is shown in Fig. 2a. In Fig. 2b thermocouples and the fiber optic are shown on the midplane, prior to assembly.

The sample is heated from the aluminum boundary by direct heating using resistive wire heaters wound around the cylinder wall and controlled by a temperature controller reading a thermocouple embedded in the aluminum at the midplane. The aluminum case inner diameter matches the HE sample diameter to provide a slip fit for good thermal contact between the walls and the sample. The endcaps are machined with a step to allow extra volume for the difference in linear thermal expansion between the HE and the aluminum, and more importantly, to allow for the ~7% volume expansion of the HMX which occurs on heating through the β–δ solid polymorphic phase transition.[6, 7]

The temperature trajectory applied is shown in Fig 3. The experiment is heated from ambient to 178 °C at 5 °C /min with a pause at 70 °C to allow a brief system check. The sample is held at 178 °C for approximately 20 minutes to allow the endothermic phase transition to occur and the internal temperatures to equilibrate. As seen in the temperature measurements made in the PBX 9501, the endothermic phase transition begins from the outer edge and progresses through the sample volume taking several minutes to complete.[2, 8] After completion of the phase transition and temperature equilibration, the sample is then heated at 5 °C /min up to the final isothermal hold point of 205 °C. At this point, the aluminum boundary is held at 205 °C and as the exothermic reactions begin to take place in the energetic material the conductive boundary begins to act as a heat sink rather than a heat source, driving the elevation of temperature into the material.[9] By pinning the boundary temperature, the hottest point in the sample is driven to the

point furthest from the conductive boundary, which is the center of the cylinder. The thermocouples placed across the midplane of the explosive are used to monitor these events *in situ*.

The isothermal region at 205 °C lasts for approximately 30 minutes before the central volume ignites.[10-12] As seen in Fig 3, the HE reaches the 205 °C boundary temperature within ~ 5 minutes, and then the heating due to exothermic reactions takes it above the boundary temperature in the "self heating" regime. As self heating progresses, the heating rate accelerates and in the final few minutes, it rises from rates of degrees per minute to tens of degrees per minute, and finally to ignition. This is called the thermal runaway regime and there is a point during the thermal runaway at which the heat is generated too fast for thermal diffusion to keep up with it so that ignition is inevitable, regardless of boundary conditions. This has been referred to as the point of no return.[13] In this regime, the central ignition volume becomes kinetically isolated from the volume around it.[14] This isolation and effective lack of diffusive heat loss leads to a temperature rise within the volume which is exponential in time. Ultimately the experiments described here end in a thermal explosion, where the consumption of solid and release of energy is believed to occur by mechanisms of subsonic burning, which completely consumes these samples in approximately 100 μs.[3] Application of necessary confinement and protection in these experiments is crucial.

## III. RESULTS AND DISCUSSION

### A. Quasistatic

The β–δ phase transition in HMX occurs, first at the case boundary, at a control temperature of 178 °C. The phase transition is endothermic and the progress of the transition can be observed

as internal temperature measurements first exhibit a slower rate of heating, and then cool during the progress of the transformation. The resulting internal structure is a complex function of the dependence of the rate of transformation on temperature, and the spatial temperature gradients which result from the energy source at the boundary and the consumption of energy by the material during transformation[1, 11]. The molar volume of the delta crystallographic phase is approximately 7% greater than in beta, and in the polycrystalline sample this expansion induces a volume increase and material flow.[7] We image this material flow and measure the resulting changes in the internal material density. During this slow thermal heating process, images are collected every minute to provide several images during the course of the transition. We refer to these frames showing the very slow evolution of the material state as quasistatic images.

### *1. Images*

The quasistatic images are taken during heating up to 205 °C. Figure 4 shows a set of images taken in the radial view where the image axis is along the cylinder axis (top panels) and in the side view where the images are taken transverse to the cylinder axis (bottom panels). The left panel is a transmission radiograph where dark correlates with low transmission and light with high transmission. The right panel is a ratio of a transmission image taken after the $\beta-\delta$ phase transition to one taken before the transition.

### *2. Image analysis*

The image ratios show the change in transmission. The images on the right of Fig. 4 are scaled so that dark represents a decrease in transmission and light an increase in transmission, both relative to the grey background indicating no change in transmission. For example the dark

vertical features in the endcap of the side view image at the bottom right of Fig. 4 indicates a decrease in transmission. This is due to the flow of material into initially empty space caused by the phase transition. This will be discussed more fully below.

Taking ratios of the images as shown in Fig. 4 enhances changes, but is also very sensitive to edges where any change in registration appears as a differential in the ratio. The vertical lines in the side view image ratio in Fig. 4 are caused by the nichrome wire heaters wrapped around the experiment changing position as the experiment heats and expands.

More quantitative analysis may be applied to these images by plotting the numerical values of the transmission along spatial axis. This is shown in Fig. 5 where the transmission ratio is plotted along the diagonal viewing down the cylinder axis. The radial flow pattern induced by the phase transition has left a density gradient of lower density at the edges and higher as the center of the cylinder is approached. This is visually apparent from the lightening and darkening in the top right image of Fig. 4.

### *3. Discussion*

As the HE undergoes the volume expanding phase transition, it expands and fills the initial void volume. This time dependence is illustrated in Fig. 6, which shows three transmission ratio images taken before, during, and after the phase transition. The ullage region in each endcap can be seen to fill during the phase transition and is evident as a dark band caused by a decrease in transmission as HE moves into the void space, as in Fig. 4. Figure 7 shows the evolution of transmission with time at three positions across the HE diameter compared to 2 regions in the aluminum endcap. The three regions in the HE all show similar trends with time, compared to the aluminum regions which are relatively constant in time. The HE regions show that at the time

of the phase transition, there is an overall decrease in transmission corresponding to an increase in scattering as the proton path length increases along the experiment axis.

From this information alone, the change in proton opacity could be caused by a combination of a material density gradient and a path length gradient. The axial images however show no path length gradient and show that the HE fills the void volume, but the HE density in this region is spatially varying with higher density at the center and lower towards the edges. Thus the phase change encodes a density gradient across the HE diameter.

Figure 8 illustrates the change in transmission for the side view images showing three regions; in the void region (yellow triangles), in the center of the HE (blue diamonds), and in a control region which should be constant in the aluminum wall (red circles). The transmission in the void drops during the phase transition when the HE volume expansion fills the void volume. The central region of the HE decreases in density and increases in transmission as the axial expansion decreases the material density. The control region tests the scatter in the measurement.

## B. Thermal runaway

Finally, during the thermal runaway regime leading to ignition, images are collected with 1 to 10Hz frequency to follow the evolution of the central ignition volume in what is called video mode. In this mode, several of the cameras with the "camera on a chip" format are used to collect frames at up to 5 Hz per camera with three cameras interleaved to provide 10 Hz imaging.[15]

### *1. Images*

Images of the thermal runaway regime are taken by running the fastest cameras at 1 to 10Hz collection rate for a predetermined number of frames. When the temperature trajectory indicates

that the central hottest region of the HE is within the final minutes before thermal explosion, the proton beam and fast cameras are started in a continuous video mode, collecting frames at a constant frequency to capture the events leading to ignition. These frames, taken at 1-10 Hz, capture the final state of the HE prior to ignition, but are not synchronized in any way with the ignition event to capture the fast dynamics of the thermal explosion. Synchronization of proton radiographs with the ignition event will be the subject of another paper.[4] Figure 9 shows final transmission images taken before the thermal explosion event for a 1" diameter (A) and a ½" diameter (B) experiment in the radial view with 3X electromagnetic magnification. The light region at the center is due to an increased transmission and decreased density in this central volume, which is the hottest region and is undergoing thermal runaway.

Figure 10 shows the preignition density evolution taken from the side view of an experiment. The top panel shows the direct transmission and the bottom panel the change in transmission. The light region in the change in transmission is the density loss which evolves in the seconds prior to ignition. It is slightly off of the midplane, and appears slightly longer axially than radially. Further work is underway to test the reproducibility of this axial elongation.

### *2. Image analysis and discussion*

The observation of decreasing density as ignition is approached is an important feature of the thermal decomposition chemistry and mechanisms of ignition in these solid explosives. For these sealed experiments the most likely hypothesis of this decreasing density is the conversion of solid to gas, which is then free to permeate the entire volume of the cylinder. The region of increased transmission is concentrated in the 1-2 mm ellipse at the center of the image and is detectable with the transmission sensitivity of these experiments. The decrease in transmission

due to the permeation of the resulting gas phase products into other regions of the image is not observed. This is consistent with a permeation of these gases throughout the volume of the case, which would dilute the decrease in transmission. It is possible that experiments with higher transmission sensitivity will be able to detect this permeation of decomposition products. We devote this last section to a full characterization of this feature for PBX 9501 subject to the thermal boundary conditions of these experiments.

The transmission profiles as a function of diameter for the two experiments of Fig. 9 are shown in Fig. 11. The two profiles as a function of diameter are very similar, and as these are two experiments of differing diameter this indicates that the central volume of reduced transmission is approximately the same size independent of the full experiment diameter. This can be understood by the notion that the exothermic processes causing the central ignition are fast enough in these final seconds that thermal and chemical diffusion away from them is no longer coupled to the walls of the cylinder, either ¼" or ½" away. The diameter of the central volume is approximately 1-2 mm. The overall transmission gradient in the final frames is higher transmission towards the center and lower towards the walls, implying a spatial density gradient opposite of that imposed on the HE during the phase transition discussed above.

Figure 12 shows the evolution of the central density gradient over the final hundred seconds for both the ½" and 1" diameter shots. It illustrates how the central density evolves in time toward explosion. In Fig. 13, the evolution of the spatial gradients in both temperature and solid density are shown. The gradients for both temperature and solid density undergo a reversal as the experiment progresses from early to late. Early on, the metal boundary is a heat source and the central volume is the coldest, whereas the final temperature distribution has very steep spatial gradients with the central volume hottest and the HE nearest the walls pinned at the lowest

temperature. Likewise, the solid density after the phase transition is highest at the center of the cylinder as shown above and lowest at the wall. As the temperature inversion occurs, the density gradient also reverses and the final density leading to ignition has a low density ignition volume developing at the center of the experiment. The extreme spatial gradients set up in temperature and in density lead to a kinetic isolation effect which we utilize to perform dynamic radiography of thermal explosions, as discussed in the companion papers.[4]

## IV. CONCLUSIONS

This paper reviews the mass flow and density changes in a PBX 9501 thermal explosion during the slow heating process and over the final seconds prior to the thermal explosion. Radiographic images showing material density are collected using proton radiography. Material motion due to thermal expansion and a polymorphic phase transition are shown. The phase transition causes the HE to expand into the void volume and imposes a density gradient across the HE with highest density towards the center of the HE. The HE is then held at a temperature at which a thermal explosion occurs within tens of minutes. The evolution of material density during the exothermic steps leading to ignition are imaged and show the reversal of the density gradient with the central volume having the lowest density. In the final seconds leading to explosion, the central volume begins to runaway and generates heat and products faster than they can be communicated to the outer walls of the case, yielding a central ignition volume with ~ 1-2 mm diameter.

## V. ACKNOWLEDGEMENTS

This research was supported by DOE Science Campaigns 1 and 2 and the NSR&D Program administered by Los Alamos National Laboratory, as well as the Joint Munitions Program administered by both the National Nuclear Security Administration and the Department of Defense.

## VI. REFERENCES

1. B. F. Henson, L. Smilowitz, B. W. Asay and P. M. Dickson, Journal of Chemical Physics **117** (8), 3780-3788 (2002).
2. L. Smilowitz, B. F. Henson, B. W. Asay and P. M. Dickson, Journal of Chemical Physics **117** (8), 3789-3798 (2002).
3. L. Smilowitz, B. F. Henson, J. J. Romero, B. W. Asay, C. L. Schwartz, A. Saunders, F. E. Merrill, C. L. Morris, K. Kwiatkowski, G. Hogan, P. Nedrow, M. M. Murray, T. N. Thompson, W. McNeil, P. Rightley and M. Marr-Lyon, Physical Review Letters **100** (22), 228301-228304 (2008).
4. L. Smilowitz, B. F. Henson, J. J. Romero, B. W. Asay, A. Saunders, F. E. Merrill, C. L. Morris, K. Kwiatkowski, G. Grim, F. Mariam, C. L. Schwartz, G. Hogan, P. Nedrow, M. M. Murray, T. N. Thompson, C. Espinoza, D. Lewis, J. Bainbridge, W. McNeil, P. Rightley and M. Marr-Lyon, Journal of Applied Physics **submitted** (2011).
5. C. Morris, J. W. Hopson and P. Goldstone, Los Alamos Science **32**, 32-44 (2006).
6. H. H. Cady, D. T. Cromer and A. C. Larson, Acta Crystallographica **16** (7), 617-& (1963).
7. M. Herrmann, W. Engel and N. Eisenreich, Propellants, Explosives, Pyrotechnics **17** (4), 190-195 (1992).
8. P. M. Dickson, B. W. Asay, B. F. Henson, C. S. Fugard and J. Wong, AIP Conference Proceedings **505**, 837-840 (2000).
9. L. Smilowitz, B. F. Henson, M. M. Sandstrom, B. W. Asay, D. M. Oschwald, J. J. Romero and A. M. Novak, AIP Conference Proceedings **845** (1), 1211-1214 (2006).
10. B. F. Henson, Asay, B. W, Dickson, P. M., Fugard, C. and Funk, D. J. , Eleventh Symposium (International) on Detonation, 325-331 (1998).
11. B. F. Henson, B. W. Asay, L. B. Smilowitz and P. M. Dickson, AIP Conference Proceedings **620**, 1069-1072 (2002).
12. B. F. Henson, L. Smilowitz, B. W. Asay, M. M. Sandstrom and J. Romero, Thirteenth Symposium (International) on Detonation, 778-785 (2006).
13. M. J. Kaneshige, A. M. Renlund, R. G. Schmitt and W. W. Erikson, 2002 (unpublished).
14. L. Smilowitz, B. F. Henson, M. M. Sandstrom, B. W. Asay and J. Romero, Thirteenth Symposium (International) on Detonation, 1026-1034 (2006).
15. K. Kwiatkowski, J. F. Beche, M. T. Burks, G. Hart, G. E. Hogan, P. F. Manfredi, J. E. Millaud, C. L. Morris, N. S. P. King, P. D. Pazuchanics and B. Turko, IEEE Transactions on Nuclear Science **49** (1, 2), 293-296 (2002).

**FIGURE CAPTIONS**

Fig. 1. Proton transmission verses sample areal density in g/cm$^2$ (top panel) and change in proton transmission verses change in areal density in g/cm$^2$ (bottom panel).

Fig. 2. (a) Schematic drawing of the 1" diameter solid cylindrical experiment. The PBX 9501 sample is shown in white and the aluminum case in grey. The sample midplane can be seen as the plane bisecting the two cylinders. (b) Picture of the midplane of one sample during construction. The aluminum case and white PBX 9501 are shown with the thermocouples and fiber optics in place on the midplane.

Fig. 3. Temperature profiles of aluminum case (black line) and internal measurements of explosive temperature (grey lines).

Fig. 4. Schematic of experiment and proton transmission images along two different orientations. The top panels are the view down the cylinder axis (radial view) with the transmission on the left and the change in transmission on the right. The bottom panels are viewing perpendicular to the cylinder axis (side view).

Fig. 5. Lineout across a radial view image showing density profile change during phase transition.

Fig. 6. Change in transmission during the $\beta-\delta$ phase transition. The darkening vertical features show the increased density at the endcaps as material flows into the ullage volume during the expansion which accompanies the transition.

Fig. 7. The panel on the right shows a radial view image and several different regions of interest. The change in transmission during the phase change in each region is shown in the left panel.

Fig. 8. The change in transmission in regions of aluminum, aluminum plus HE, and ullage measured in side view during the phase transition.

Fig. 9. Central ignition volume in a 1" diameter (A) and ½" diameter (B) experiment. The view is down the cylinder axis in direct transmission, with the transmission scale shown at the right of the figure.

Fig. 10. Side on image of the density evolution in the final seconds leading to ignition. The top panel shows the transmission image, the bottom the change in transmission. Line profiles across the central region are shown right of and below the images. The light region near the center is where solid density is being lost as the ignition volume sets up.

Fig. 11. Transmission line profiles showing the central region of density loss for the ½" and 1" diameter experiments taken in the seconds before ignition occurs.

Fig. 12. The change in transmission as a function of time, integrated over the central ignition volume for seconds leading to ignition. Data in red and black are for the ½" and 1" diameter experiments, respectively.

Fig. 13. Top: Transmission ratio profiles for five times spanning approximately 20 s before ignition, plotted as a function of the diameter in the view down the cylinder axis. Bottom: Same view, now plotting the measured internal temperatures at the midplane as a function of diameter for the same 20 s period preceeding ignition.

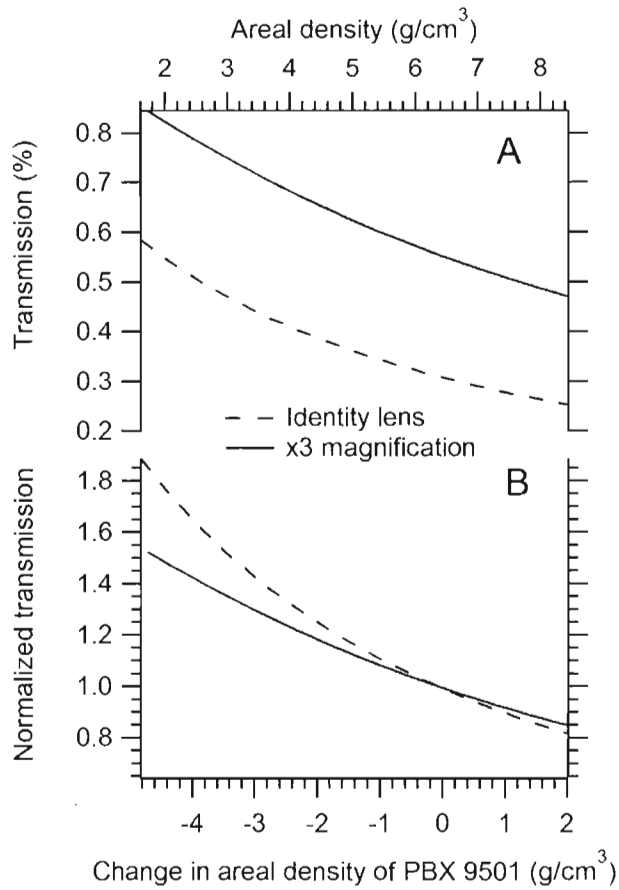


Figure 1: Smilowitz et al.

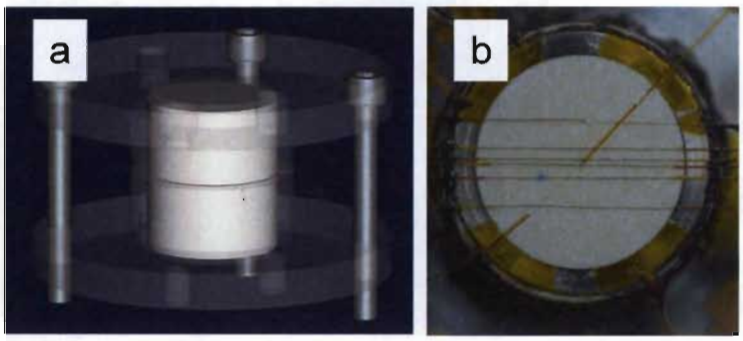


Figure 2: Smilowitz et al.

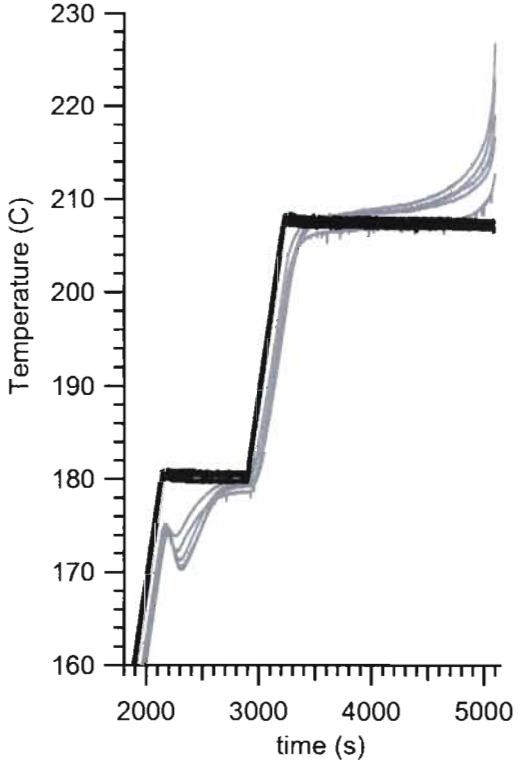


Figure 3: Smilowitz et al.

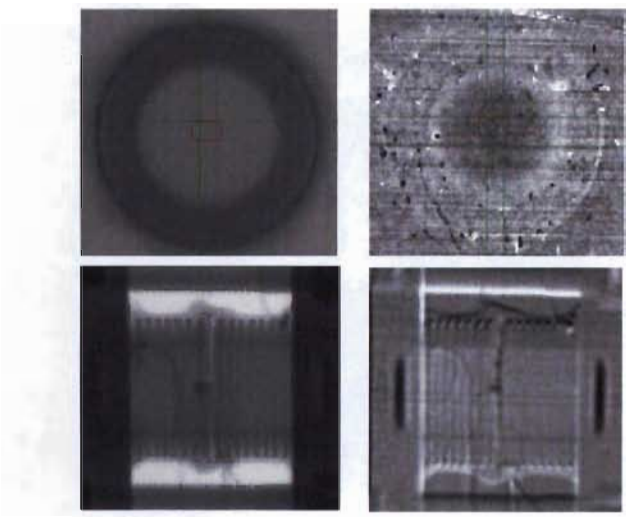

Figure 4: Smilowitz et al.

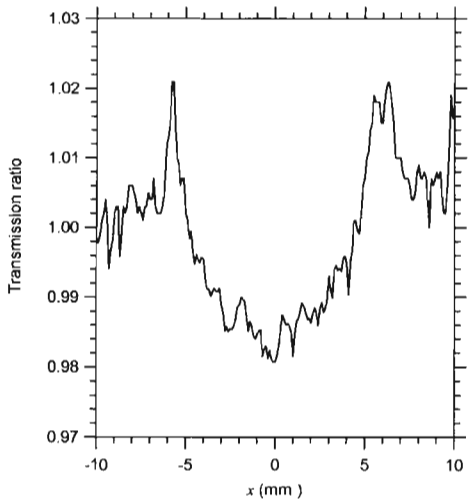


Figure 5: Smilowitz et al.

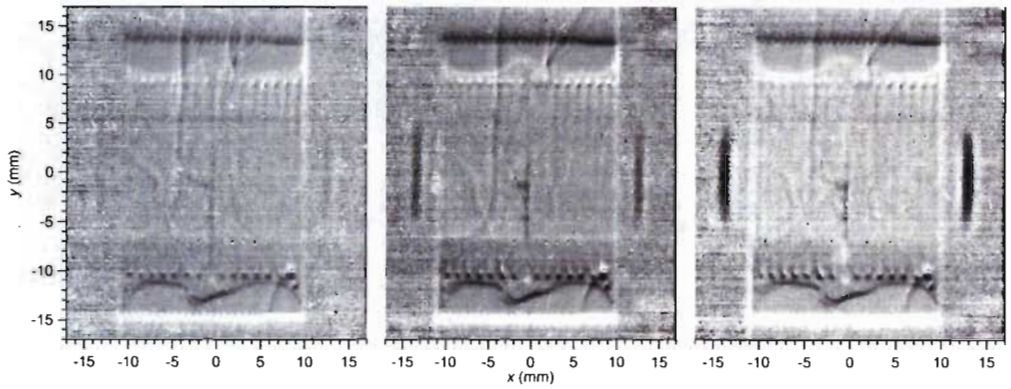


Fig. 6: Smilowitz et al.

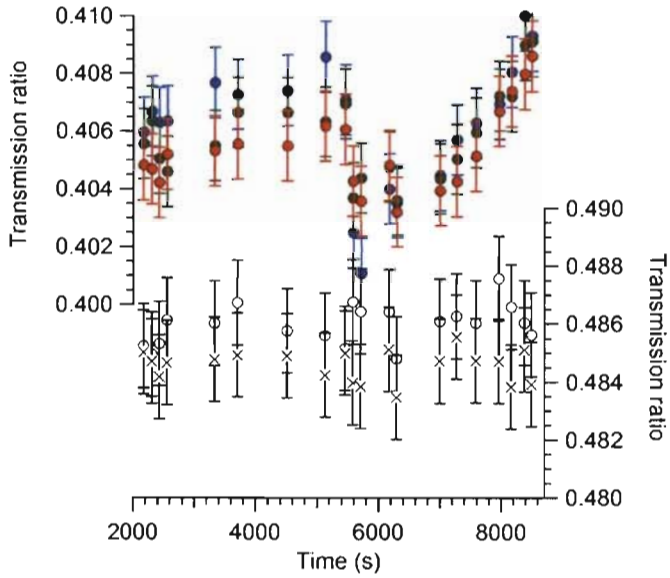


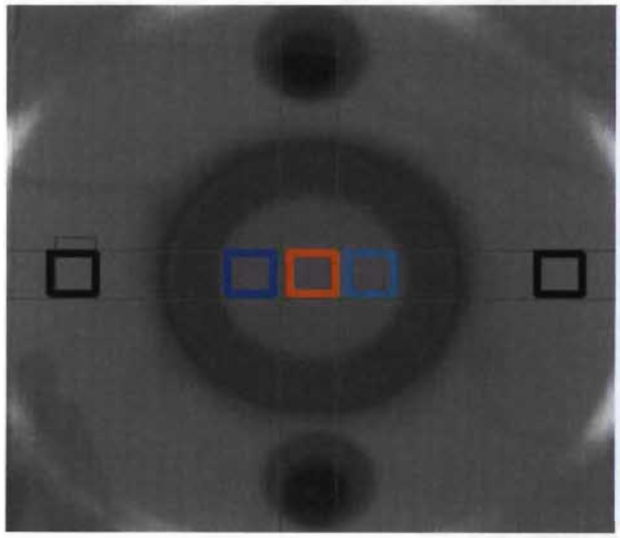

Figure 7: Smilowitz et al

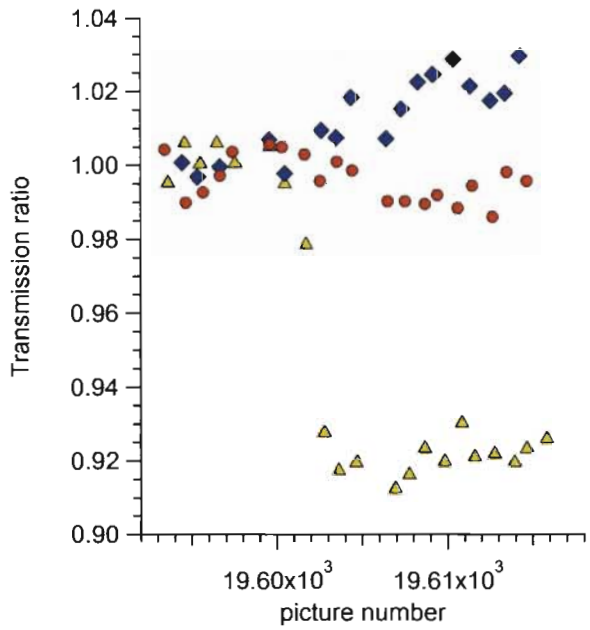


Figure 8: Smilowitz et al.

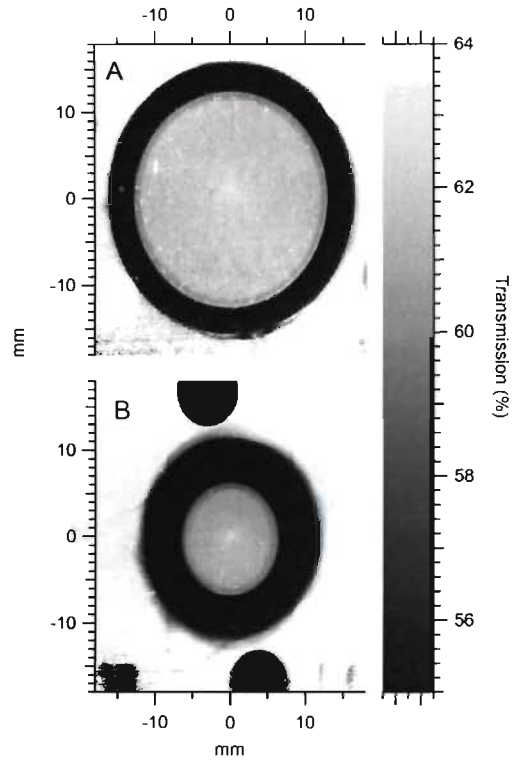


Figure 9: Smilowitz et al.

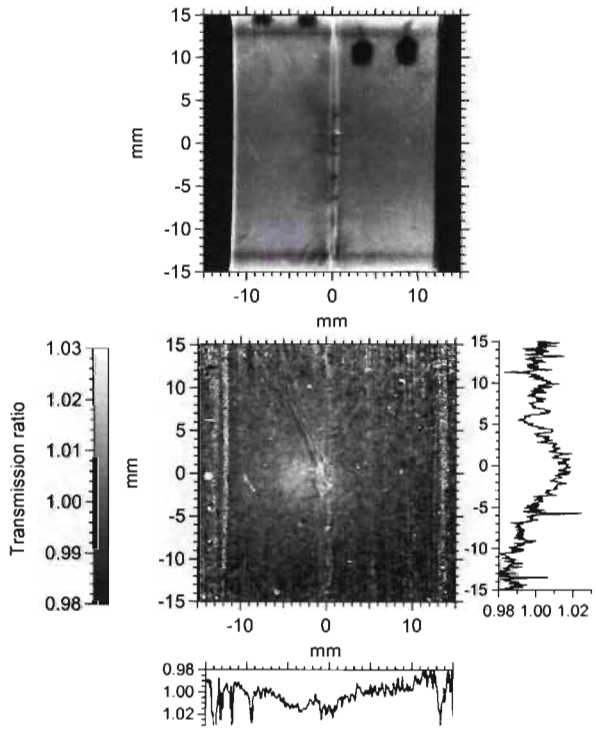


Figure 10: Smilowitz et al.

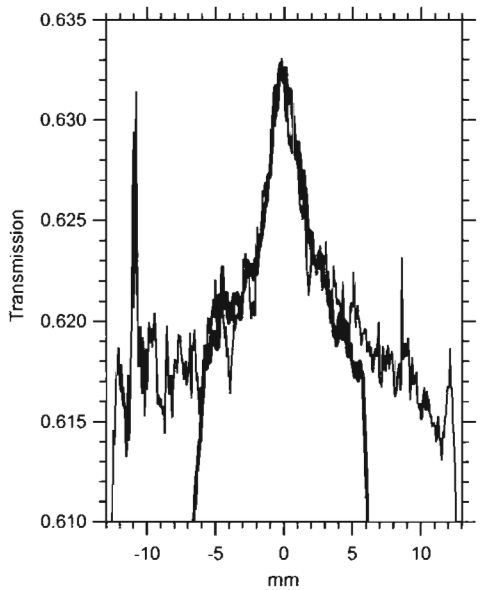


Fig 11: Smilowitz et al.

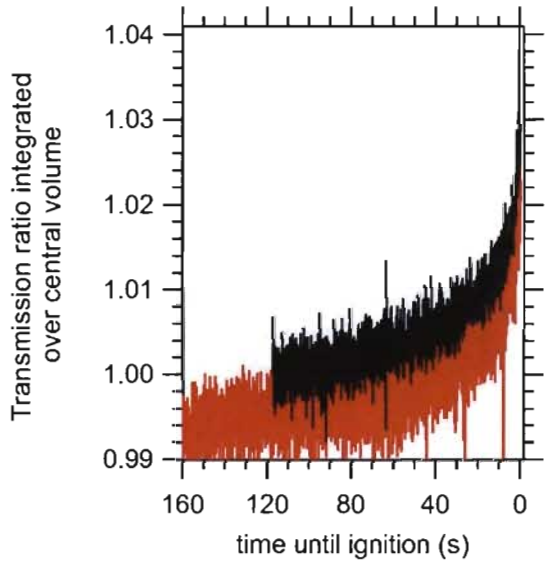


Figure 12: Smilowitz et al.

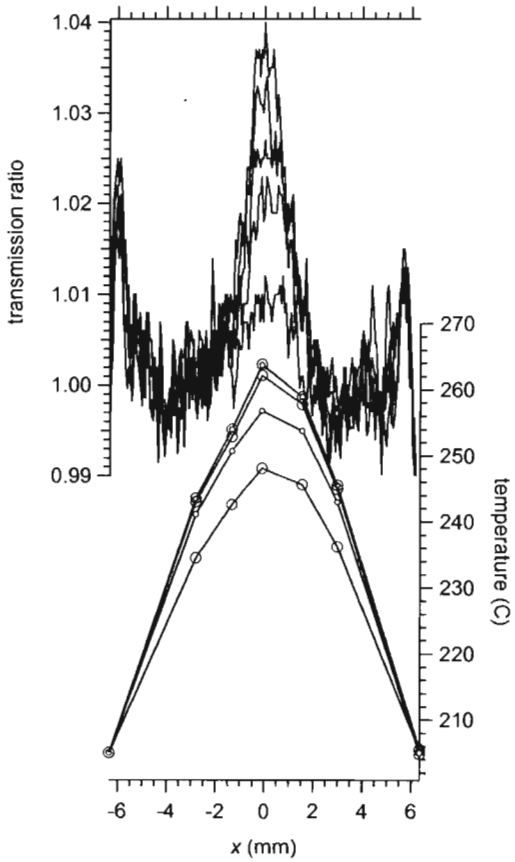


Figure 13: Smilowitz et al.